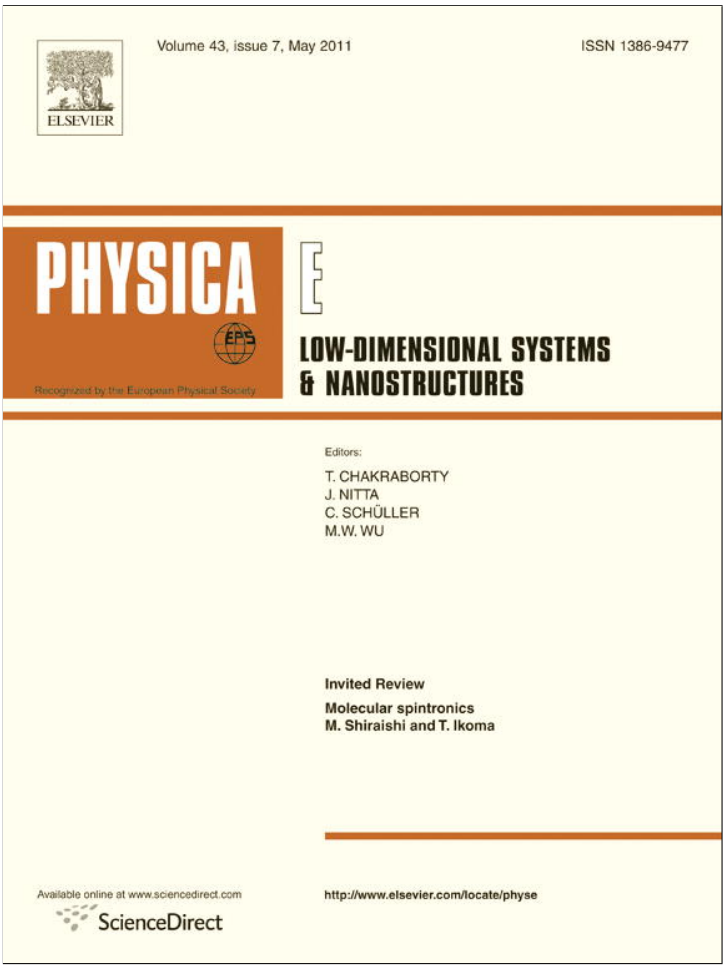

Physica E 43 (2011) 1351–1359

Contents lists available at ScienceDirect

Physica E

journal homepage: www.elsevier.com/locate/physe

First principles calculations of C_{70} fullerene nano-cage doped with transition metal atoms (Fe, Co)

M. Bezi Javan, N. Tajabor*, M.Rezaee Roknabadi, M. Behdani

Department of Physics, Faculty of Sciences, Ferdowsi University of Mashhad, Mashhad, Iran

ARTICLE INFO

Article history:
Received 1 December 2010
Received in revised form
25 February 2011
Accepted 8 March 2011
Available online 29 March 2011

ABSTRACT

Total energy calculations of the C_{70} fullerene nano-cage doped with transition metals, (TM=Fe and Co atoms), endohedrally, exohedrally, and substitutionally were performed using density functional theory with the generalized gradient approximation along 18 different paths inside and outside of the fullerene. The most stable structures were determined with full geometry optimization near the minimum of the binding energy curves of all the examined paths. The results reveal that for all stable structures, the Co atom has a larger binding energy than the Fe atom. It is also found that for all complexes additional peaks contributed by TM-3d, 4s, and 4p states appear in the highest occupied molecular orbital (HOMO) and the lowest unoccupied molecular orbital (LUMO) gap of the host cluster. The mid-gap states are mainly due to the hybridization between TM-3d, 4s, and 4p orbitals and the cage π orbitals. The magnetic moment of endohedrally and exohedrally doped Fe and Co atoms in the C_{70} fullerene are preserved to some extent due to the interaction between the TM and C atoms of the cage, in contrast to the completely quenched magnetic moments of the Fe and Co atoms in the C_{69}TM complex. Furthermore, Mulliken charge population analysis shows that overall charge transfer occurs from TM atom to the cage.

1. Introduction

Fullerenes have attracted considerable interest since the discovery of C_{60}. A promising area of research concerns metal–fullerene interactions and their application to advanced nano-materials, with potential use in optical and magnetic devices.

So far numerous experimental studies for endohedrally doped [1–7] or exohedrally doped [8–10] fullerenes with metal atoms have been undertaken by resorting to arc-desorption or laser vaporization techniques. On the other hand, it has become possible to synthesize the heterofullerenes, where the foreign atom is incorporated into the carbon cage.

In the past several years, some work has been done on the doping of C_{60} and C_{70} using transition metals [11–14] because of their valence level structure, such as ns, (n−1)d, and (n−2)f, which may exhibit different spin configurations. On the other hand some first principle density functional investigations have been reported earlier on TM–C_{60} nano-clusters [15,16].

Fullerene C_{70} as the second most abundant fullerene and its derivatives have attracted some attention in various fields, from pharmaceuticals to materials science. The C_{70} fullerene, which is larger than C_{60}, has a larger binding energy per atom than C_{60} [17]. However, it has been found that some of the C_{70} sites have larger reaction energies than that of the C_{60} [18]. Billas et al. [19] reported that the stable structure of exohedrally doped fullerene C_{70} with Fe and Co atom can be produced in a low pressure condensation cell, through the mixing of a vapor of the doping material with a vapor made of fullerene C_{70}. They have also synthesized heterofullerene C_{69}TM (TM=Fe and Co) with stable structures.

To the best of our knowledge, there is no comprehensive theoretical investigation on the TM–C_{70} complexes. It seems that more studies are needed to get better understanding of the properties of TM–C_{70} systems and hence to predict their potential applications. In this work we studied structural, electronic, and magnetic properties of endohedral, exohedral, and substitutional doped fullerene C_{70} (D5h) with transition metals (TM=Fe and Co), which are appropriate candidates for designing magnetic devices if high spin configuration can be preserved as the ground state or different spins manipulated.

2. Computational details

To simulate the endohedral, exohedral, and substitutionally doped fullerene with the TM atom first principle approaches using numerical atomic orbitals as a basis set have been implemented. Full geometrical optimization and total energy calculations were performed with *ab initio* calculations based on the generalized

* Corresponding author. Tel./fax: +98 511 8763647.
E-mail address: ntajabor@yahoo.com (N. Tajabor).

1386-9477/$ - see front matter © 2011 Elsevier B.V. All rights reserved.
doi:10.1016/j.physe.2011.03.005

gradient approximation (GGA) with the Perdew–Burke–Erenzerhof (PBE) functional [20] in the density functional theory and the standard norm-conserving Troullier–Martins pseudopotentials [21]. We have used the openMX code that is based on the linear combination of pseudo-atomic orbital (LCPAO) basis functions for solving the standard Kohn–Sham equations and has been demonstrated to be very efficient for large atomic systems [22–24]. In the calculations with openMX, the same outer electrons of the TM atom were treated as valence electrons in the self consistent field iteration. The pseudo-atomic orbitals have been constructed using a basis set (two-s, two-p, two-d for TM and two-s and two-p for C) within 7.0 Bohr radii of the cutoff radius for confinement potential of the TM and 5.0 Bohr radii for the C atom. The cutoffs of 150 Ry for the grid integration were utilized to represent the charge density in the real space. The structure of C_{70} is more complicated than that of C_{60}. The 10 additional atoms at the equator generate five additional hexagonal rings and lower the symmetry of the fullerene to D5h, resulting in five nonequivalent atoms and eight different bonds. To find the most stable structure of endohedral and exohedral doped fullerenes we have performed single point energy calculations. We devise 18 inner and outer different paths. Each inner path starts from the cage center and is extended to one of the symmetric key points on the surface of the C_{70} cage, such as different atomic sites ("A"–"E"), midpoint of the different bonds ("B1"–"B8") and center of the hexagonal and pentagonal rings ("C1"–"C5"). The optimized geometry of D5h C_{70} is shown in Fig. 1 with eighteen nonequivalent key points on its surface. We refer to each path with the same designated name to the key point to which the path ends. Each external path starts from infinity toward one of the key points. For endohedral and exohedral TM-doped fullerenes, the binding energy variation is studied as a function of distance between the TM atom and the center or the surface of the cage, respectively. The binding energy is taken as the total energy of each complex minus the sum of the total energies of the cage and the free TM atom at infinite separation. The geometric structure of the complexes relaxed near the minimum of the binding energy by Hellman–Feynman forces, including Pullay-like corrections. Structural optimizations were performed using the conjugate gradient algorithm until the residual forces were smaller than 0.01 eV/Å. For the heterofullerene complexes the stable geometry was obtained directly by the full geometry optimization. It was shown by previous theoretical studies [25–28] that the structure of C_{60} predicted by the DFT-GGA method is in good agreement with experiment, hence reinforcing the reliability of the theoretical method used in the present study. Using this theoretical approach, the calculated bond lengths of C_{60} are 1.425 and 1.402 Å for single, (5–6), and double, (6–6), bonds, respectively. These are also in agreement with the experimental values [25,27]. The calculated bond lengths of the D5h C_{70} in LCPAO theory have been compared with different theoretical calculations and experimental values in Table 1. As it is clear the LCPAO results are in good agreement with the GGA-BLYP theoretical calculations [28] and that of the experimental results [27].

3. Results and discussions

3.1. Geometric structure

3.1.1. TM@C_{70} (TM=Fe, Co)

The change in the binding energy of TM atoms with respect to the internal surface of the C_{70} cage was calculated. Binding energies along all the 18 selected paths were computed as a function of the distance from the cage center, and some results for the Fe@C_{70} case are shown in Fig. 2. As can be seen from Fig. 2(a) a local minimum of the binding energy with value of −0.3 eV is at the center of the cage. When the Fe atom leaves the center toward the inner surface of the C_{70} cage on the different paths, which end at the different atomic sites, the binding energy reaches the maximum negative value at distance of 0.65, 1.29, and

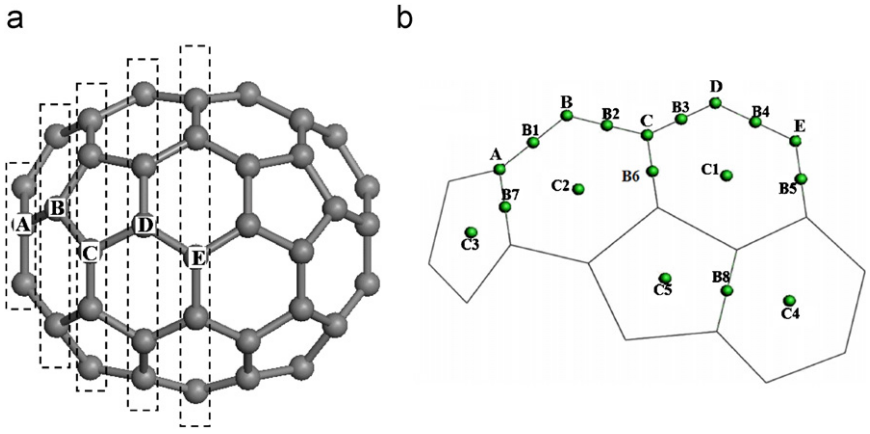

Fig. 1. Optimized D5h C_{70} (a) and the 18 different more symmetric key points on the C_{70} surface (b); the ("A"–"E"), ("B1"–"B8"), and ("C1"–"C5") sets refer to the different atomic sites, middle of the bonds, center of the hexagonal and pentagonal rings, respectively.

Table 1
Structural characteristics of the C_{70} fullerene.

C_{70}								
Bond	A–A	A–B	B–C	C–C	C–D	D–D	D–E	E–E
Number of bonds	10	10	20	10	20	10	20	5
LCPAO	1.452	1.403	1.449	1.395	1.450	1.434	1.423	1.463
GGA–BLYP [28]	1.458	1.404	1.454	1.398	1.452	1.444	1.427	1.477
LDA [28]	1.439	1.39	1.436	1.384	1.434	1.427	1.411	1.455
Experimental [27]	1.460	1.382	1.449	1.396	1.464	1.420	1.415	1.477

Bond lengths are in Å. The corresponding sites are labeled in Fig. 1.

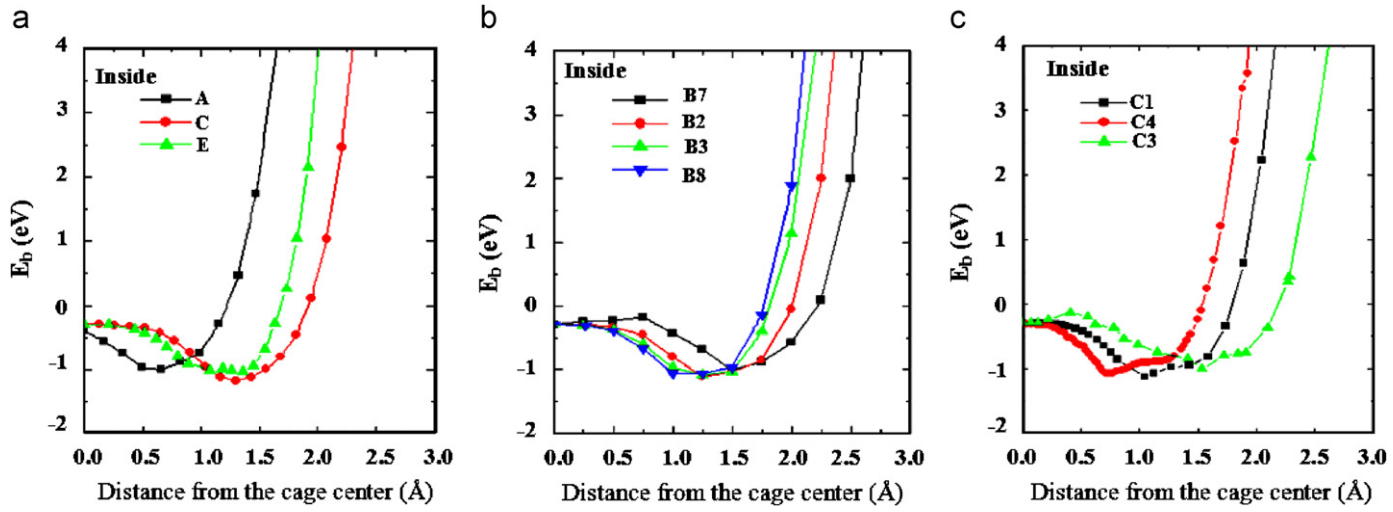

Fig. 2. Variation of the binding energy with distance of the Fe atom from the cage center on some selected paths which end at (a) different atomic sites, (b) middle of the different bonds, and (c) midpoint of the different hexagonal and pentagonal rings.

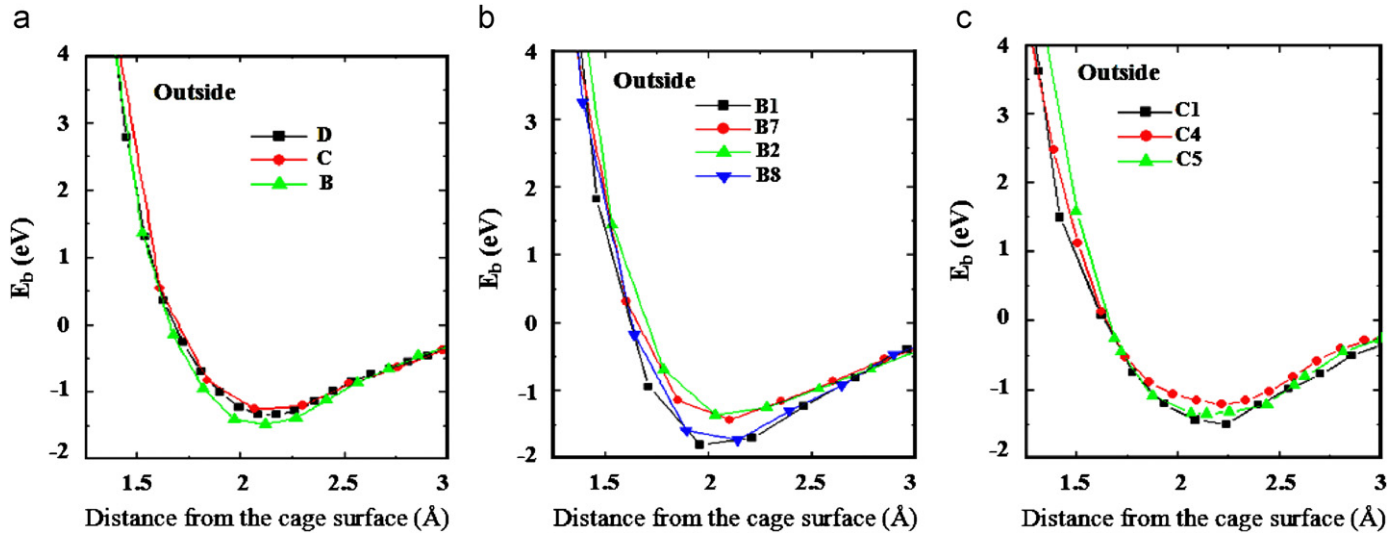

Fig. 3. Variation of the binding energy with distance of the Fe atom from the cage surface on some selected paths which start from infinity and end at (a) different atomic sits, (b) middle of the different bonds, and (c) midpoint of the different hexagonal and pentagonal rings.

1.26 Å from the cage center for the selected paths A, C, and E, respectively. The global minimum of the binding energy is on the C path at 1.29 Å from the cage center with the value of −1.23 eV. For some selected paths that are directed to the middle of different bonds the binding energy curves are shown in Fig. 2(b). As is clear, the cage center in all cases is a local minimum of the binding energy curves. The global minima of the binding energy curves for B3 and B7 are at 1.5 Å and for the other paths the minima occur at 1.24 Å from the cage center with the value of −1.11 eV. This is the most negative value of the binding energy in this set. Fig. 2(c) shows the variation of the binding energy curves on the C1, C3, and C4 paths, which end to the midpoint of the different hexagonal and pentagonal rings. The global energy minima of these paths occur at 0.73, 1.52, and 1.04 Å from the cage center, respectively. The minimum of the binding energy in these radial paths is related to the C4 path with the value of −1.15 eV.

As is revealed the minimum of the binding energy among all the examined paths is related to the C path. After full geometry optimization of the Fe@C_{70} structure near the minimum of the binding energy curve, the distance of the Fe atom changes from 1.29 to 1.32 Å from the cage center with the binding energy of −1.24 eV, which indicates that the inner most stable site of the Fe atom is below the carbon atom of the cage, which is denoted by the "C" site. By a similar geometric optimization process for the Co atom inside the C_{70} cage, the optimized distance of the Co atom is obtained at 1.13 Å from the cage center along the C path with the binding energy of −1.35 eV. The negative binding energy of the endohedrally doped TM (Fe and Co) atom in the C_{70} cage indicates that the complexes have thermodynamically stable structures. Also it can be seen that the absolute value of the binding energy of the Co atom is about 0.11 eV higher than that of the Fe atom.

The calculated Fe–C and Co–C bond lengths are 2.59 and 2.73 Å, respectively. For both endohedrally doped TM atoms in the C_{70} cage the TM–C bond lengths are longer than the sum of the TM and C atomic radii so their interaction can be of ionic nature. The symmetry of the TM@C_{70} is C1, which is lower than the D5h for C_{70} case.

3.1.2. *TM:C_{70} (TM=Fe, Co)*

The binding energy variations of the Fe atom approaching the outer surface of the cage in some different paths are shown in Fig. 3.

It is clear from Fig. 3(a) that when the Fe atom comes from infinity toward the outer surface of the C_{70} cage along the B, C, and D paths, the binding energy has a minimum on each path. The minima of the C and D paths occur at 2.07 Å from the cage surface in the range −1.26 to −1.37 eV. The minimum of the binding energy of the Fe atom on the B path appears at 2.12 Å from the cage surface with the value of −1.49 eV, which is the most negative value of the binding energy in this series. The binding energy variations of the Fe atom along four selected paths among B1 to B8 are shown in Fig. 3(b). It can be seen that the binding energy minimum on the B1 path appears at 1.96 Å from the cage surface with the most negative value of 1.80 eV. The difference between this and the other binding energy values for B2–B8 paths are about 0.41, 0.56, 0.33, 0.75, 0.05, 0.33, and 0.19 eV. Some selected binding energy curves for straight paths that are directed from infinity to the middle of the different hexagonal and pentagonal rings are shown in Fig. 3(c). It is found that the global energy minima of the C1–C5 paths occur at 2.23, 2.08, 2.22, 2.24, and 2.06 Å from the cage surface and the minimum of the binding energy in these five different paths is related to the C1 path with the value of −1.53 eV.

According to the above results the most negative value of the binding energy among all the 18 examined outer paths is related to the B1 path. After full geometrical optimization of the Fe:C_{70} structure near the minimum of the binding energy, the distance of the Fe atom changes from 1.94 to 1.92 Å from the cage surface with the binding energy of −1.86 eV, which indicates that the outer most stable site of the Fe atom is above the A–B bond of the cage. By a similar geometric optimization process for the Co atom outside the C_{70} cage, the optimized distance of the Co atom is obtained at 1.84 Å from the cage surface along the B1 path with the binding energy of −2.98 eV. The negative binding energy of the exohedrally doped TM (Fe and Co) atom in the C_{70} cage is an indication that the complexes have thermodynamically stable structures. Also it can be seen that the binding energy of the Co atom to the cage is about 1.12 eV higher than that of the Fe atom.

The calculated Fe–C and Co–C bond lengths are 2.28 and 1.98 Å, respectively. For exohedrally doped Fe atom on the C_{70} cage the Fe–C bond lengths are longer than the sum of the Fe and C atomic radii so their interaction can be of ionic nature but for exohedrally doped Co atom on the C_{70} cage the Co–C bond lengths are shorter than the sum of Co and C atomic radii so their interaction can be of ionic and covalent nature. The TM:C_{70} complex also has the C1 symmetry, which is lower than that of the C_{70} case.

3.1.3. $C_{69}TM$ (TM=Fe, Co)

In order to explore the stable structure of the C_{69}TM we have optimized all the five possible geometries where the carbon atom can be replaced by the TM atom. The binding energy variations of the C_{69}Fe and C_{69}Co complexes are shown in Fig. 4 for different occupations of the atomic sites "A"–"E" of the C_{70} cage by the TM atom. The binding energy is defined as the absolute value of the difference between the total energy of the complexes and the energy sum of the 70 free atoms constituting the structure of the complexes, which is the essential standard of estimating thermodynamic stability of a complex. One can see that $C_{69}Fe^A$ and $C_{69}Co^A$ isomers are more stable than the other isomer of the C_{69}TM. Also the binding energies of all C_{69}Co isomers are higher than those of C_{69}Fe isomers. The binding energies of the relaxed structures of $C_{69}Fe^A$ and $C_{69}Co^A$ are 0.91 and 0.85 eV/atom, respectively, which are smaller than that of C_{70}. These results indicate that the TM–C bond in C_{69}TM is weaker than the C–C bond in C_{70} structure. The modification of the bond lengths are confined mainly to the TM–C bonds with bond lengths much greater than the corresponding C–C bond length of C_{70} as shown in Table 2. The magnitude of the deformation induced by the Fe atom is somewhat greater than that induced by the Co atom on-cage substitution. The reason is that the Fe atomic radius is somewhat greater than that of the Co atom [29].

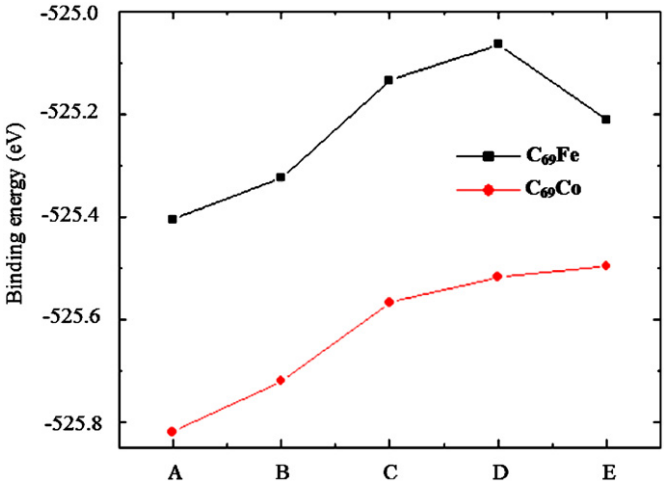

Fig. 4. Binding energy variations of the C_{69}Fe and C_{69}Co complexes when different atomic sites "A"–"E" of the C_{70} cage are occupied by the TM atom.

Table 2
Bond lengths (in Å) of C_{69}Fe and C_{69}Co calculated in this work.

Bonds	$C_{69}Fe^A$	$C_{69}Co^A$
$Fe–C^A$	1.973	
$Fe–C^B$	1.856	
$Co–C^A$		1.929
$Co–C^B$		1.850
A–A	1.462	1.455
A–B	1.410	1.416
B–C	1.463	1.451
C–C	1.405	1.409
C–D	1.449	1.450
D–D	1.431	1.435
D–E	1.422	1.425
E–E	1.458	1.456

3.2. Vibrational frequencies

To insure that geometry optimization is realized properly, calculation of vibrational frequencies has been performed using DFT with PBE exchange-correlation functional theory. The obtained un-scaled infrared (IR) intensities versus vibrational frequencies are shown in Fig. 5. The absence of any imaginary vibrational frequency confirms that all the examined structures correspond to the true minima of the potential energy hyper surface and the optimized structures are stable.

3.3. Electronic and magnetic properties

Now we discuss the effect of the dopant atoms on the electronic structure of the C_{70} fullerene. A general feature is that all dopants introduce states in the gap between the highest occupied molecular orbital and the lowest unoccupied molecular orbital (HOMO–LUMO gap) of the fullerene. First we discuss the density of states (DOS) of the most stable complexes mentioned above. In Fig. 6 we have plotted the total DOS (gray line) and the partial density of states (PDOS) on the TM-3d, 4s and 4p orbitals (red, green, and blue curves,

respectively) for up (α) and down (β) spins. The vertical dashed line in each figure shows the HOMO (or Fermi level, E_f) of the complex. The Gaussian broadening has been used while plotting the DOS curves and the HOMO level was shifted to zero. The DOS of the C_{70} cage for comparison with those of the other complexes is shown in Fig. 6. It is found that for the considered complexes, additional peaks contributed by the TM-atomic orbitals appear in the HOMO–LUMO gap of the host cluster. From PDOS, it is clear that the mid-gap states are mainly due to the hybridization between TM-3d, 4s, and 4p orbitals and the cage π orbitals. At a glance a deformation can be recognized in the DOS, including in-shape and shift toward the lower energy region compared with the DOS of the C_{70} cage. This substantial shift can be explained by growth of the effective coulomb potential due to the charge transfer from dopant atom to the cage. Furthermore, the DOS and PDOS in Fig. 6 show typical magnetic features of the considered complexes. For the Fe@C_{70} system the HOMO level is in the β state and mainly localized on the Fe-3d orbital, while the LUMO level is in the β state and composed from 0.18Fe-3d+0.82C-2p orbitals hybridization. According to the PDOS analysis obtained for the ground state of the exohedrally Fe-doped C_{70} complex, the α-HOMO level contains 0.35Fe-4 s+0.18Fe-4p+0.47C-2p while the β-LUMO level is composed of 0.09

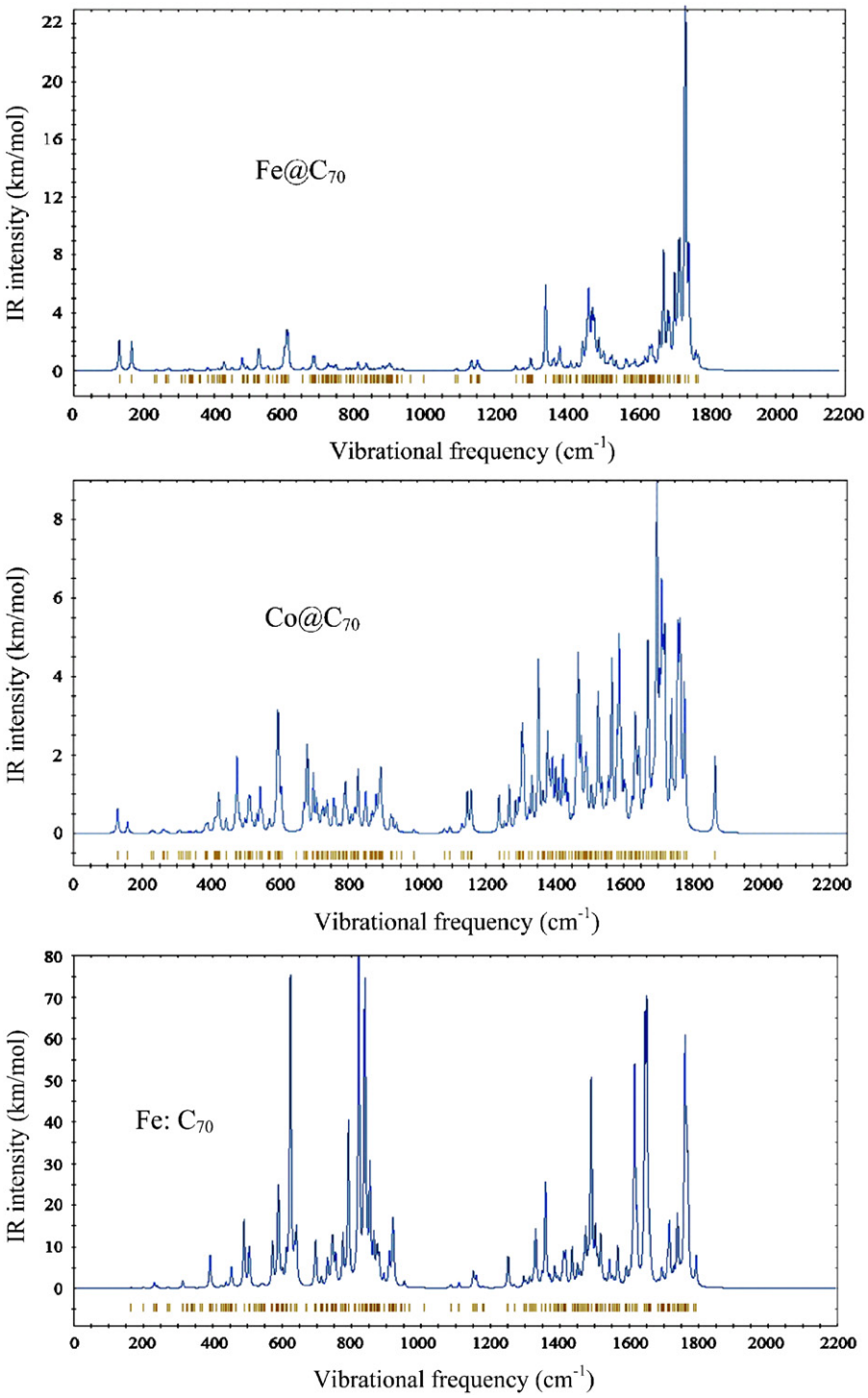

Fig. 5. Simulated IR spectrum of Fe@C_{70}, Co@C_{70}, Fe:C_{70}, Co:C_{70}, C_{69}Fe, and C_{69}Co complexes.

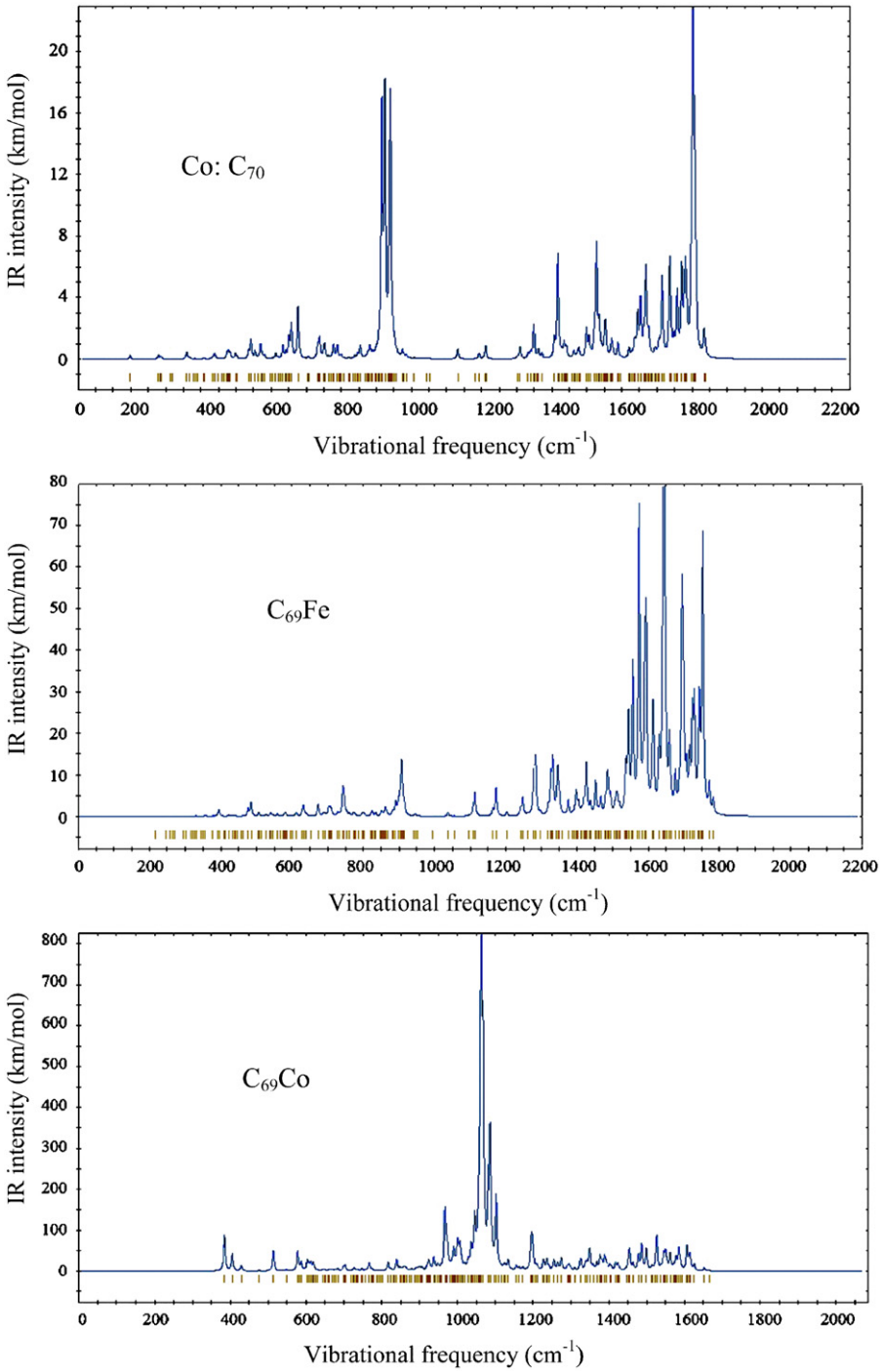

Fig. 5. (*Continued*)

Fe-4s+0.43Fe-3d+0.48C-2p orbitals. In the case of the $C_{69}Fe$ heterofullerene, the α- and β-HOMO and LUMO are degenerate; therefore they have the same energies. In this case the HOMO and LUMO are composed of 0.75Fe-3d+0.25C-2p and 0.01Fe-4s+0.36Fe-3d+0.08Fe-4p+0.55C-2p orbitals, respectively. We find that the HOMO of $Co@C_{70}$ is in the β state and composed of 0.88Co-3d+0.12C-2p while its LUMO is in the α state and contains none of the Co atomic orbitals. For the $Co:C_{70}$ complex the β-HOMO and α-LUMO are composed of 0.23Co-4 s+0.69Co-3d+0.08C-2p and 0.21Co-4 s+0.11Co-4p+0.68C-2p orbitals, respectively. Also in $C_{69}Co$ heterofullerene the HOMO and LUMO are composed of 0.29Co-3d+0.05Co-4s+0.08Co-4p+0.61C-2p and 0.30Co-3d+0.13Co-4p+0.57C-2p orbitals, respectively. The HOMO and LUMO isosurfaces of the most stable complexes considered in this work are shown in Fig. 7. The HOMO, LUMO, and HOMO–LUMO gaps for all configurations are given in Table 3. The HOMO of the $Fe@C_{70}$ is 1.430 eV higher in energy than the HOMO of C_{70}, thus the ionization is more easily realized. The LUMO of $Fe@C_{70}$ is 0.041 eV lower in energy than the LUMO of C_{70}, so the extra electron enters the LUMO of $Fe@C_{70}$ easily. Since the HOMO energies are recognized as an indicator of the first ionization potential (IP), the order of the first IP of the complexes is as follow: $Co:C_{70} > Co@C_{70} > Fe:C_{70} > Fe@C_{70} > C_{69}Fe > C_{69}Co > C_{70}$. Also the LUMO energies are sometimes considered as an approximation to the electron affinities (EA). So the order of the first EA of these complexes is as follow: $C_{69}Co > C_{69}Fe > Fe:C_{70} > Fe@C_{70} > C_{70} > Co@C_{70} > Co:C_{70}$. The different nature of hybridization

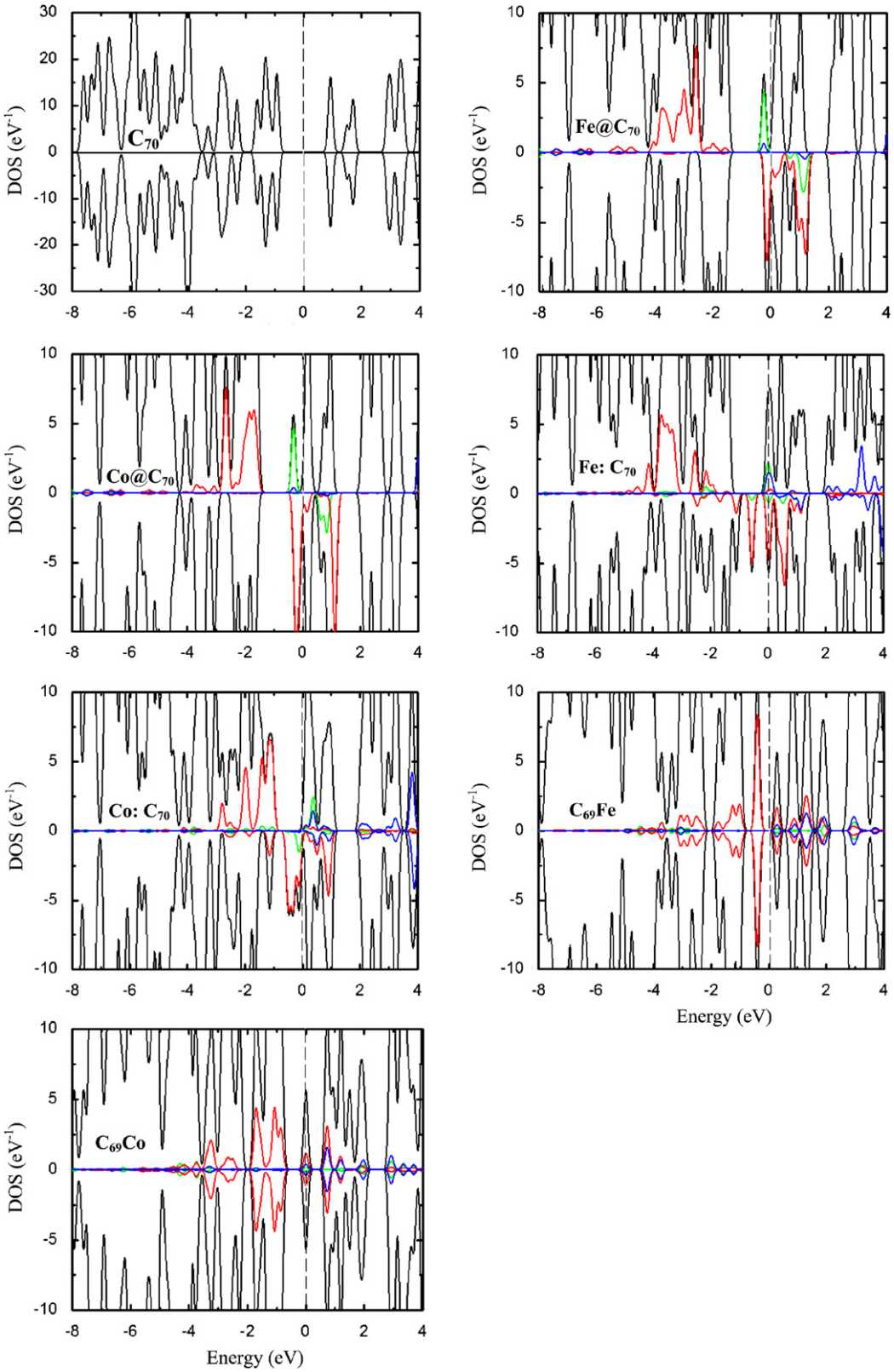

Fig. 6. DOS of C_{70}, Fe@C_{70}, Co@C_{70}, Fe:C_{70}, Co:C_{70}, C_{69}Fe, and C_{69}Co systems. The light gray, green, red, and blue curves refer to the complex, TM-4s, 3d, and 4p orbital PDOS. The vertical dashed line in each figure shows the Fermi level of the complex, which is shifted to zero point.

between the TM-atomic orbitals and the C-2p orbital is well reflected in the magnitude of the local magnetic moment on the TM atom, in Table 4. We also show the total magnetic moment and the Mulliken charge population of TM valence orbitals. It can be seen that the total magnetic moment of the systems for Fe@C_{70}, Fe:C_{70}, and C_{69}Fe are essentially close to the magnetic moment of the dopant atom with small magnetic moment induced on the cage in all cases. In the case of Fe@C_{70} and Fe:C_{70}, an anti-parallel magnetic moment of $0.379\mu_B$ and a parallel magnetic moment of $0.025\mu_B$ are induced on the cage, respectively. In the case of Co@C_{70} and Co:C_{70} anti-parallel magnetic

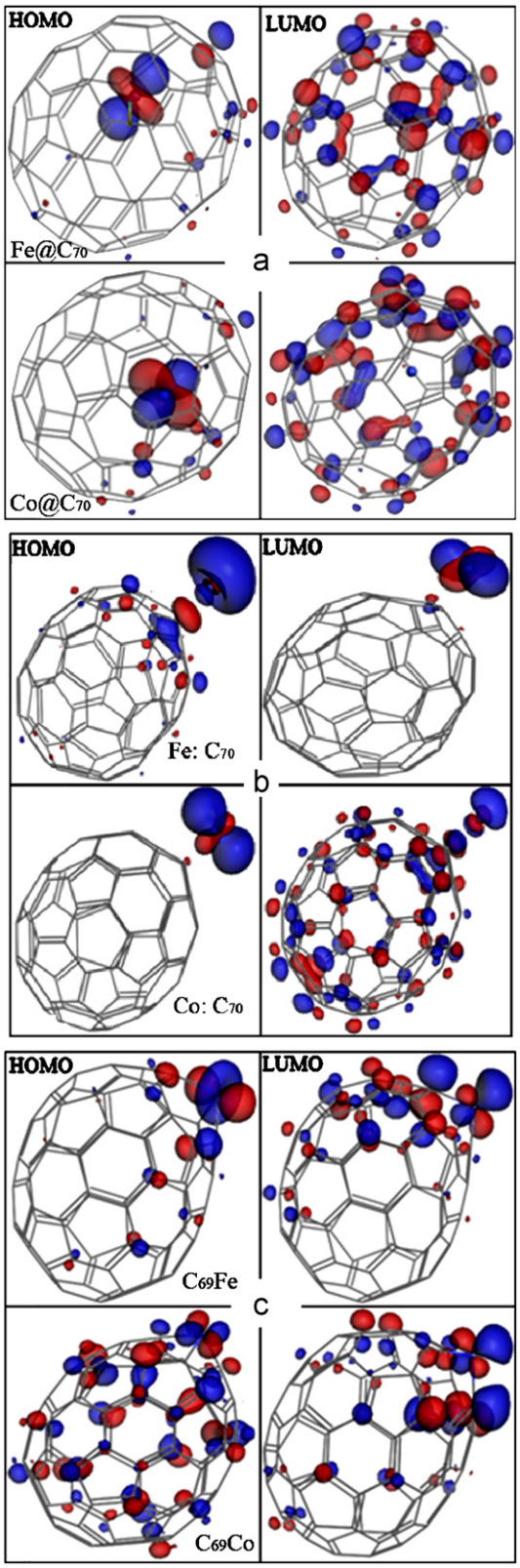

Fig. 7. HOMO and LUMO of (a) TM@C_{70}, (b) TM:C_{70}, and (c) C_{69}TM systems.

moments of 0.174 and 0.269μ_B induced on the cage decrease the total magnetic moment of the systems. We can see from Table 4 that the zero net spin population of the TM atom in C_{69}TM preset the completely quenched magnetic moment of the TM atom in the C_{69}TM heterofullerene.

Table 3
HOMO, LUMO, and HOMO–LUMO gap of the complexes and its orbital spin state (spin up (α) and spin down (β) states).

Complexes	HOMO (eV)	LUMO (eV)	*Eg*
C_{70}[a]	−5.563	−3.839	1.724
Fe@C_{70}	−4.133 (β)	−3.880 (β)	0.253
Co@C_{70}	−4.043 (β)	−3.806 (α)	0.237
Fe:C_{70}	−4.054 (α)	−4.019 (β)	0.035
Co:C_{70}	−3.899 (β)	−3.662 (α)	0.237
C_{69}Fe[a]	−4.767	−4.101	0.666
C_{69}Co[a]	−5.379	−4.541	0.838

[a] HOMO and LUMO orbitals of the structure are doubly degenerate by up and down spin states.

Table 4
Magnetic properties and Mulliken population analysis of the dopant atoms.

Complex	Total magnetic moment	TM (μ_B)	3d (μ_B)	4s (μ_B)	4p (μ_B)	
Fe@C_{70}	4	4.379	3.415	0.811	0.153	
Fe:C_{70}	3.786	3.761	3.192	0.370	0.199	
C_{69}Fe	0	0	0	0	0	
Co@C_{70}	3	3.174	2.242	0.840	0.092	
Co:C_{70}	1	1.269	1.434	−0.146	−0.019	
C_{69}Co	0	0	0	0	0	
TM atom Mulliken Spin population	Spin up			Spin down		
Analysis	3d	4s	4p	3d	4s	4p
Isolated Fe atom	5	1	0	1	1	0
Fe@C_{70}	5.099	0.924	0.298	1.684	0.113	0.145
Fe:C_{70}	4.923	0.662	0.330	1.731	0.292	0.131
C_{69}Fe	3.477	0.408	0.215	3.477	0.408	0.215
Isolated Co atom	5	1	0	2	1	0
Co@C_{70}	5.114	0.955	0.234	2.872	0.115	0.142
Co:C_{70}	4.731	0.350	0.128	3.297	0.496	0.147
C_{69}Co	3.932	0.438	0.267	3.932	0.438	0.267

The key point to the magnetic moment behavior in all examined structures is the charge depletion of the TM-4s orbitals due to the confinement and hybridization. As it can be seen from Table 4 the enhancement of charge population in the minority TM-3d orbital that comes from 4s charge depletion determines the total magnetic moment of the systems in all cases. The TM-4s orbital charge depletion in Fe@C_{70}, Fe:C_{70}, and C_{69}Fe is 48%, 52%, and 59%, respectively. Also for Co@C_{70}, Co:C_{70}, and C_{69}Co the 4s charge depletion is 46%, 58%, and 56%. The direction of charge transfer between the dopant atom and the carbon cage appears to be determined by their relative electronegativity. As the C atom is more electronegative than the TM atom the electronic charge transfers from the TM to the carbon cage. Since the Fe atom transfers part of its electron to the nearest-neighbor carbon sites it has net positive charge of 0.263e and 0.069e in Fe@C_{70} and Fe:C_{70} complexes, respectively. In the case of C_{69}Fe heterofullerene the net charge on Fe atom is almost 0.2e. The electronic configurations of the Fe atom in Fe@C_{70}, Fe:C_{70}, and C_{69}Fe complexes are [Ar] $3d^{6.783}$ $4s^{1.037}$ $4p^{0.443}$, [Ar] $3d^{6.654}$ $4s^{0.954}$ $4p^{0.461}$, and [Ar] $3d^{6.954}$ $4s^{0.816}$ $4p^{0.430}$, respectively. Like the Fe atom in Fe–C_{70} systems, the Co atom transfers part of its electron to the nearest-neighbor carbon sites; it has appreciable net positive charge of 0.432e and 0.149e in Co@C_{70} and Co: C_{70} complexes, respectively. In C_{69}Co system the net charge on the Co atom is almost 0.274e. In the case of the

Co–C_{70} systems the electronic configurations of the Co atom in Co@C_{70}, Co:C_{70}, and C_{69}Co complexes are [Ar] $3d^{7.986}4s^{1.070}$ $4p^{0.376}$, [Ar] $3d^{8.028}$ $4s^{0.846}$ $4p^{0.275}$, and [Ar] $3d^{7.864}$ $4s^{0.876}$ $4p^{0.534}$, respectively.

4. Conclusions

In summary, our first principle results show that the transition metal atoms Fe and Co may form stable structures with the C_{70} fullerene. The full geometry optimization near the minimum of the binding energy curves shows that the most stable position of the Fe and Co atoms in the TM@C_{70} system is below the "C" labeled atomic site of the C_{70} cage. Also the most stable position of both Fe and Co atoms in TM:C_{70} complex is above the "B1" labeled bond. For all examined structures, the Co atom has larger binding energy than the Fe atom. For all complexes additional peaks contributed by TM-3d, 4 s and 4p states appear in the HOMO–LUMO gap of the host cluster. The mid-gap states are mainly due to the hybridization between TM-3d, 4s and 4p orbitals and the cage π orbitals. The magnetic moment of the endohedrally and exohedrally doped Fe and Co atoms in C_{70} fullerene are preserved to some extent due to the interaction between TM and carbon atoms of the cage, in contrast to the completely quenched magnetic moment of the Fe and Co atoms in the C_{69}TM cage. As the C atom is more electronegative than the TM atom overall charge transfer occurs from TM atoms to the carbon cage.

References

[1] Y. Chai, T. Guo, C. Jin, R.E. Haufler, L.P.F. Chibante, J. Fure, L. Wang, J.M. Alford, R.E. Smalley, J. Phys. Chem. 95 (1991) 7564.
[2] R.D. Johnson, M.S. Devries, J. Salem, D.S. Bethune, C.S. Yannoni, Nature 355 (1992) 239.
[3] J.H. Weaver, Y. Chai, G.H. Kroll, C. Jin, T.R. Ohno, R.E. Haufler, T. Guo, J.M. Alford, J. Conceicao, L.P.F. Chibante, A. Jain, G. Palmer, R.E. Smalley, Chem. Phys. Lett. 190 (1992) 460.
[4] H. Shinohara, H. Sato, M. Ohkohchi, Y. Ando, T. Kodama, T. Shida, T. Kato, Y. Saito, Nature 357 (1992) 52.
[5] M. Takata, B. Umeda, E. Nishibori, M. Sakata, Y. Saitot, M. Ohno, H. Shinohara, Nature 377 (1995) 46.
[6] W. Sato, K. Sueki, K. Kikuchi, K. Kobayashi, S. Suzuki, Y. Achiba, H. Nakahara, Y. Ohkubo, F. Ambe, K. Asai, Phys. Rev. Lett. 80 (1998) 133.
[7] M. Saunders, Science 271 (1996) 2693.
[8] L.M. Roth, Y. Huang, J.T. Schwedler, C.J. Cassady, D. Ben-Amotz, B. Kahr, B.S. Freiser, J. Am. Chem. Soc. 113 (1991) 6298.
[9] Y Huang, B.S. Freiser, J. Am. Chem. Soc. 113 (1991) 9418.
[10] S.W. McElvany, J. Phys. Chem. 96 (1992) 4935.
[11] Y. Liang, Z. Shang, X. Xu, X. Zaho, J. Mol. Struct.: (Theochem.) 728 (2005) 225.
[12] C. Ray, M. Pellarin, J.L. Lermé, J.L. Vialle, M. Broyer, X. Blase, P. Mélinon, P. Kéghélian, A. Perez, Phys. Rev. Lett. 80 (1998) 5365.
[13] J.L. Fey, M.F. Jarrold, J. Phys. Chem. A 101 (1997) 1836.
[14] T. Ohtsuki, K. Ohno, K. Shiga, Y. Kawazoe, Y. Maruyama, K. Masumoto, J. Chem. Phys. 112 (2000) 2834.
[15] C.M. Tang, K.M. Deng, J.L. Yang, X. Wang, Chin J. Chem. 24 (2006) 1133.
[16] M.B. Javan, N. Tajabor, M. Behdani, M. Rezaei-Roknabadi, Physica B 405 (2010) 4937.
[17] S. Saito, A. Oshiyama, Phys. Rev. B 44 (1991) 11 532.
[18] Y. Ueno, S. Saito, Physica E 40 (2007) 258.
[19] I.M.L. Billas, W. Branz, N. Malinowski, F. Tast, M. Heinebrodt, T.P. Martin, C. Massobrio, M. Boero, M. Parrinello, Nanostruct. Mater. 12 (1999) 1071.
[20] J.P. Perdew, K. Burke, M. Ernzerhof, Phys. Rev. Lett. 77 (1996) 3865.
[21] N. Troullier, J.L. Martins, Phys. Rev. B 43 (1991) 1993.
[22] T. Ozaki, Phys. Rev. B 67 (2003) 155108.
[23] T. Ozaki, H. Kino, Phys. Rev. B 69 (2004) 195113.
[24] T. Ozaki, H. Kino, Phys. Rev. B 72 (2005) 045121.
[25] O.V. Pupysheva, A.A. Farajian, B.I. Yakobson, Nano Lett. 8 (2008) 767.
[26] K. Hedberg, L. Hedberg, D.S. Bethune, C.A. Brown, H.C. Dron, R.D. Johnson, M. Devries, Science 254 (1991) 410.
[27] A.V. Nikolaev, T.J.S. Dennis, K. Prassides, A.K. Soper, Chem. Phys. Lett. 223 (1994) 143.
[28] S.M. Lee, R.J. Nicholls, D. Nguyen-Manh, D.G. Pettifor, G.A.D. Briggs, S. Lazar, D.A. Pankhurst, D.J.H. Cockayne, Chem. Phys. Lett. 404 (2005) 206.
[29] J.A. Dean Lange's, Handbook of Chemistry, McGraw-Hill, New York, 1999.